Received: 13 September 2022 | Revised: 25 May 2023 | Accepted: 28 May 2023

DOI: 10.1111/ter.12670

RESEARCH ARTICLE

Terra Nova WILEY

Red or green: Overprinting of the climatic signal in Miocene sediments, South China Sea (IODP Expedition 368, Site U1502)

E. C. Ferré[1] | S. Satolli[2] | H. Wu[3] | P. Persaud[4] | D. Çukur[5] | S. A. Bowden[6]

[1]School of Geosciences, University of Louisiana at Lafayette, Lafayette, Louisiana, USA

[2]Dipartimento di Ingegneria e Geologia, Università degli Studi G. D'Annunzio di Chieti-Pescara, Chieti, Italy

[3]School of Ocean Sciences, China University of Geosciences, Beijing, China

[4]Department of Geosciences, University of Arizona, Tucson, Arizona, USA

[5]Korea Institute of Geoscience and Mineral Resources, Daejeon, Republic of Korea

[6]School of Geosciences, University of Aberdeen, Aberdeen, UK

Correspondence
E. C. Ferré, School of Geosciences, University of Louisiana at Lafayette, Lafayette, Louisiana, USA.
Email: eric.ferre@louisiana.edu

Funding information
Chinese 111; ECORD; Korean IODP; National Science Foundation; Natural Environment Research Council; U.S. Science Support Program, Lamont-Doherty Earth Observatory

Abstract

Sedimentary beds of alternating red and green colour are commonly interpreted to reflect orbitally-forced cyclic climatic, syn-depositional conditions, although colour changes caused by post-depositional fluids are also documented. Results from IODP Hole U1502A marine sediments in the South China Sea exemplify post-depositional reducing fluid–rock interactions that locally changed the sediment colour from red to green. Petrographic, rock magnetic and paleomagnetic data on cores show that the red colouration originates from an early, basin-wide, pervasive diagenetic oxidation event (forming haematite), whereas the green colouration results from subsequent fluid-driven reduction (forming pyrrhotite-magnetite). The dense sulfidic stockwork in the basaltic basement underlying these sediments was the likely source of reducing fluids. Drilling deep holes into marine basin basements can thus provide useful information on fluid transfer from the basement to the overlying sedimentary layers.

KEYWORDS
hydrothermal, IODP, Miocene, sediments, South China Sea

1 | INTRODUCTION

The South China Sea (SCS) formed during the mid- to late-Cenozoic along the rifted margin of Southeast Eurasia (Figure 1a). International Ocean Discovery Program (IODP) Expedition 367/368/368X aimed to unravel the history of continental breakup in a young continental margin and to compare this evolution with that of other nonvolcanic or magma-poor rifted margins. The expedition recovered some of these mid- to late-Cenozoic sediments (Larsen, Jian, et al., 2018; Larsen, Mohn, et al., 2018). IODP Hole U1502A from Expedition 368 provides opportunities to investigate how sediments are affected by rift-related processes. Hole U1502A encountered late Eocene to late-Miocene sediments down to 747.20 m and the flanks of a basaltic basement high, down to 920.95 m (Figures 1b and S1). The sediments alternate between grey-green and brownish-red colours between 440 and 660 m, whereas above and below they are dominantly brownish-red (Figure 2). Jin et al. (2020) interpreted these colour alternations to reflect orbitally-forced rhythmic cycles of in situ oxidized and reduced environments due to deep-sea circulation and here we propose an alternate interpretation.

2 | IODP HOLE U1502A SEDIMENTARY LITHOLOGIES

Hole U1502A encompasses Plio-Pleistocene to late Oligocene (27–5 Ma) deep marine sediments from 375.00 to 749.01 m (Figures 1b and S1), and overly hydrothermally altered and brecciated basalts (Jian et al., 2018).

Six units/subunits were observed (Jian et al., 2018). Unit I (late Miocene to late Oligocene) includes five subunits. Subunit IA (375.00 to 486.82 m) is comprised of dark grey, to greenish grey clays intercalated with brownish clays. Subunit IB (490.20–599.57 m) consists of alternating intervals of brown and greenish-grey clay and silt, with rare sandy intervals. Subunit IC (599.57–602.39 m) consists of greenish-grey and reddish-grey clayey siltstone/sandstone with parallel lamination and convolute bedding. Subunits IA–IC show several fining-upward intervals, interpreted as turbidites, of greenish-grey colour. Subunit ID (602.39–724.03 m) consists of alternating greenish and brownish clay with silt (Cores 368-U1502A-25R through 32R). Subunit IE (724.03–734.87 m) consists of brown clay with pale green haloes around fractures. Unit II (727.96–728.04 m) consists of altered, green-grey clasts of reworked basaltic material. Unit III (739.10–739.16 m) consists of a brownish-yellow, hardened, poorly sorted Fe-hydroxide-rich siliceous breccia. Unit IV (739.16–747.20 m), consists of diatom, sponge spicule, and radiolarian-rich silty clay with

Significance Statement

This manuscript provides an innovative and alternative explanation for the origin of red and green beds in marine sequences. These results are transformative because such colour alternations had been previously interpreted as reflecting orbitally-forced rhythmic cycles rather than local conditions. These results will interest communities in marine geosciences, palaeomagnetism and sedimentology. This interpretation contradicts previous views on the South China Sea.

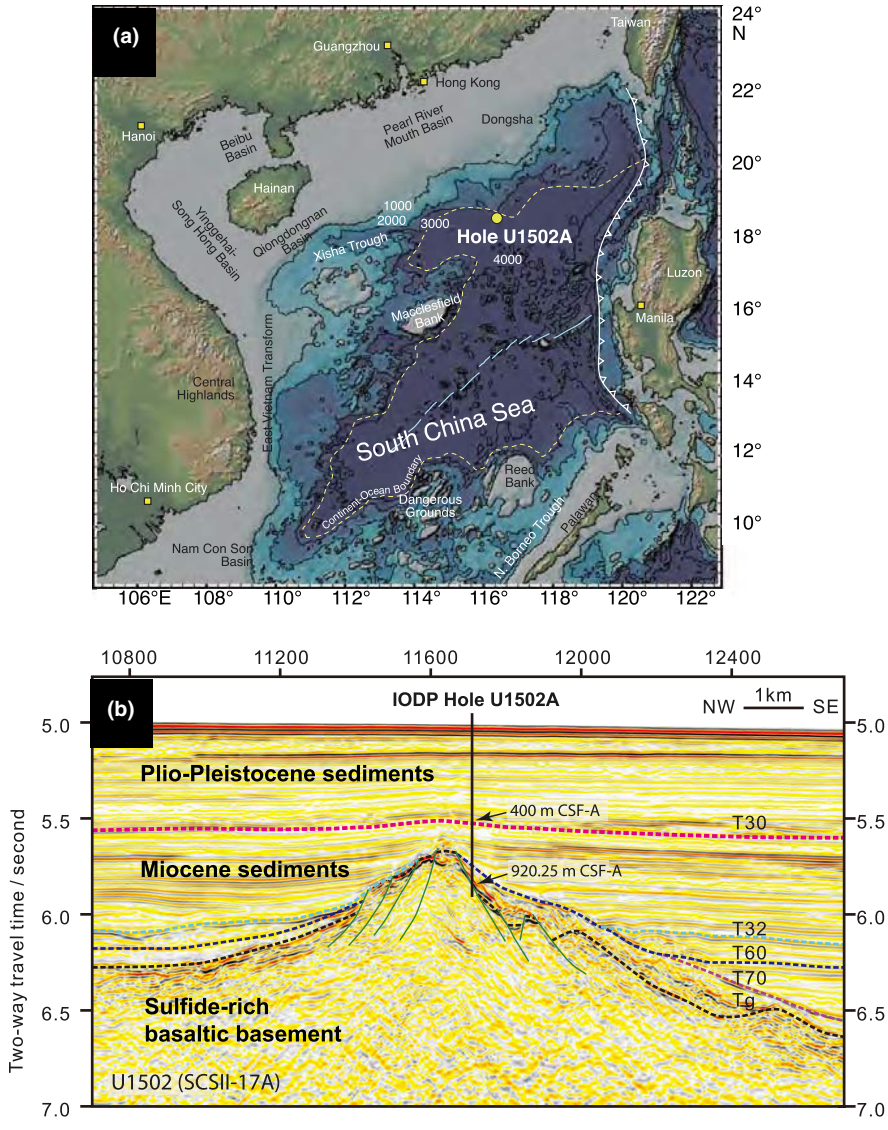

FIGURE 1 (a) Location of IODP Hole U1502A in the South China Sea. Blue segments show the spreading centres (after Pautot et al., 1986; Briais et al., 1993). (b) NW-SE seismic profile that crosses the location of IODP Hole U1502A on the SE flank of a basement high composed of basaltic rocks cross-cut by a network of sulfide veins. Coloured dash lines represent unconformities: Tg, T70, T60, T32 and T30 represent seismic unconformities. Tg: basement unconformity; T70: ~32 Ma breakup unconformity; T60: ~23 Ma regional basin event (after Larsen, Mohn, et al., 2018).

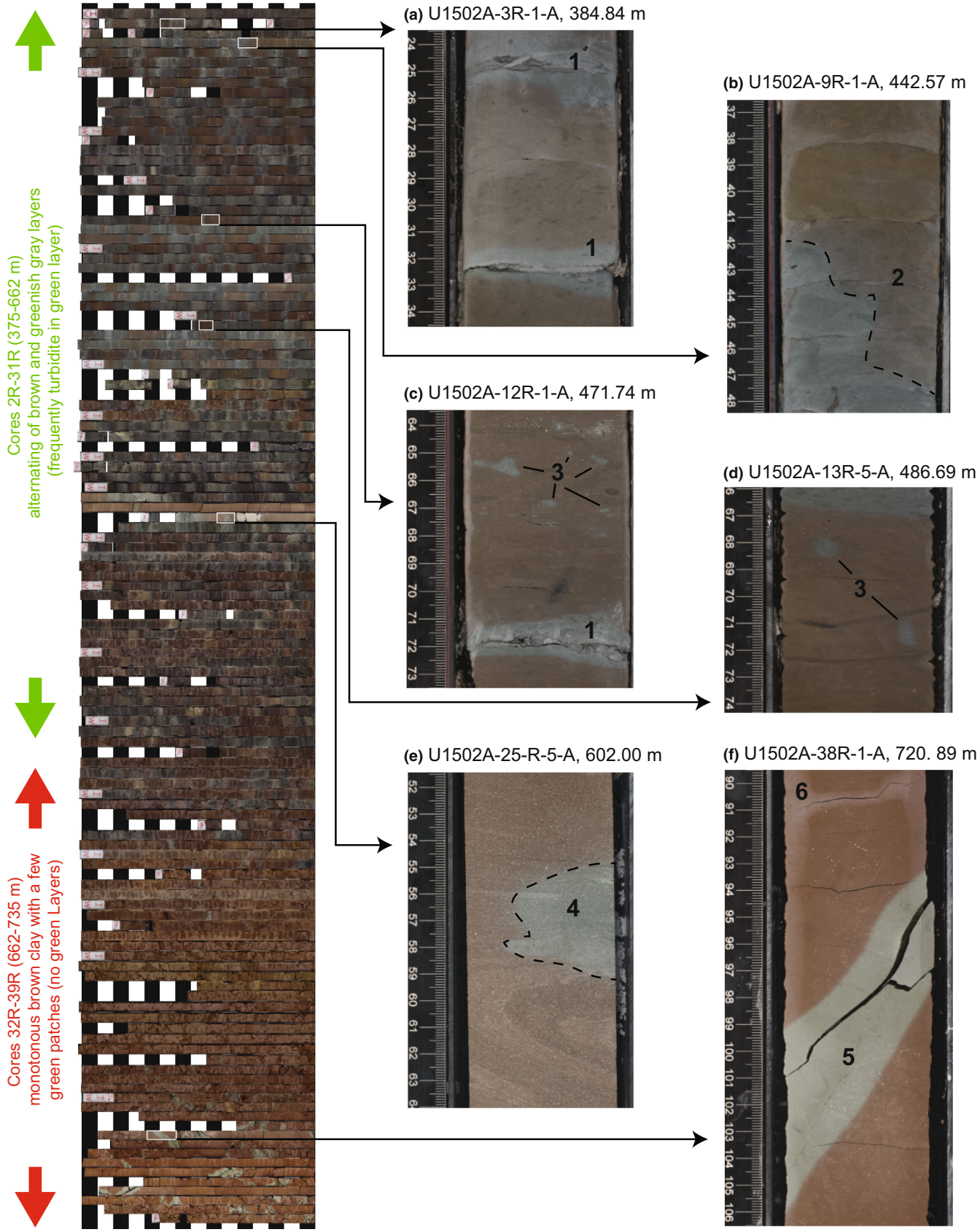

FIGURE 2 Left. Top to bottom overview of cores recovered from Hole U1502A. Right (a–f): Details of the split cores. The boundaries between green and red material cut through bedding and can occasionally be diffuse. (1) Green colour across coarser-grained laminae and fractures. (2) Gradational green-red boundary. (3) Green reduction spots form around small sulfide aggregates. (4) Green reduction overprinting sedimentary slump folds. (5) Green reduction along a fracture. (6) Discoloration of red along a fracture. White numbers indicate depth at the top of the piece.

cm-size patches of pyrite and pyrite-filled fractures. Unit V (747.20–749.01 m), consists of alternating dolomitic marble and clast-rich clay, interpreted as slightly metamorphosed sediments. This unit is partially overprinted by a high-temperature hydrothermal fluid. Unit VI (749.01–920.95 m) consists of highly altered basalt.

The sedimentary cores recovered at IODP Hole U1502A show colour variation. At 384.84 m depth (Figure 2a), the light green to grey colour correlates spatially with subhorizontal fractures and sandy laminae interpreted as turbidites, while the rest of the material preserves its original light brown colour. At 442.57 m depth (Figure 2b), the rock shows a gradational transition from brownish-red to light green-grey with an irregularly shaped boundary between colours, at a high angle to the bedding plane. Another example is shown at 602.00 m depth (Figure 2e). At 486.69 m depth (Figure 2d), light green reduction spots, <1 cm in length, occur in an otherwise brownish-red sedimentary material. Similar light green-grey reduction spots and high permeability zones associated with sandy turbidite intervals occur in many other parts of the core (Figure 2c). Finally, at 720.89 m depth (Figure 2f), the core shows a brownish-red colour, except along the core margins and small fractures where the colour is paler. Because this slight discolouration follows the core margin, it probably results from reduction by drilling fluids. Yet, the same piece shows light green-grey haloes along fractures.

3 | DOWNHOLE PARAMETERS

Downhole variations in grain size and composition of sediments provide information on the environment of deposition. Yet, fluid–rock interactions, during or after diagenesis, may modify the rock colour to the point where this colour no longer represents syn-depositional redox conditions. To better understand these interactions, we analysed macroscopic sediment colour against five parameters (Figure 3): green/red reflectance ratio (G/R ratio, dimensionless), porosity (%), magnetic susceptibility (MS in 10^{-6} [SI]), natural remanent magnetization (NRM in A/m), and NRM inclination (°). The magnetic declination is not provided because the core was not azimuthally oriented. Additional details are in Larsen, Jian, et al. (2018). Core U1502A-9R-1 (top at 442.20 m) shows the correlations between colour, G/R ratio, porosity, magnetic susceptibility, and NRM (Figure 3a). Colour variations correlate well with the G/R ratio, showing a bimodal distribution between green and red intervals (Figure 3a). Most high porosity sections correlate with green intervals. In Core 368-U1502A-9R1, MS is higher in the red sediments (average $221 \pm 52 \times 10^{-6}$ SI) than in the green sediments ($163 \pm 32 \times 10^{-6}$ SI) (Figure 3a). MS is also relatively higher in the red intervals compared to the green intervals immediately above and below. In contrast, the NRM intensity is not only higher in the green intervals than in the surrounding red intervals, but also more variable. Finally, the green intervals display different NRM inclinations polarities and absolute values compared to the beds immediately above and below. The most striking correlation is between the G/R ratio and MS. The G/R reflectance ratio and NRM intensity also show a strong correlation. In summary, throughout Hole U1502A, the magnetic assemblage of the red beds differs from that of the green beds (details in Jian et al., 2018).

4 | MAGNETIC ASSEMBLAGES

In the following, we report on twenty 2-cm cubes of green and red sediment collected between 442.86 and 742.99 m depth and present detailed results for one representative core (Core 368-U1502A-9R1). Isothermal remanent magnetization (IRM) acquisition experiments were conducted on 14 cubes up to 1.5 T, and MaxUnmix was used for deconvolution (Maxbauer et al., 2016). Alternating field (AF) demagnetization of NRM of 10 cubes was performed up to 120 mT. Finally, stepwise thermal demagnetization of a three-axis imparted IRM was performed on 8 cubes (Lowrie, 1990) up to 660°C.

The IRM deconvolution shows that 2 to 3 phases contribute to remanence and that the red sediment has a more coercive assemblage than the green. The slower rate of IRM acquisition of the red sediment indicates the presence of a high coercivity phase such as haematite (Figure 3b). In contrast, the green sediments reach saturation below 0.4 T, which points to the presence of low coercivity phases such as magnetite or pyrrhotite. Higher S-ratios, i.e., soft IRM/hard IRM ($IRM_{-0.3T}/IRM_{2.5T}$; Liu et al., 2012) in the green samples, between 0.51 and 0.90, indicate a predominance of the soft component, while in the red and mixed colour samples, S-ratios, between 0.03 and 0.30 and between 0.01 and 0.46, respectively, point to a hard component. The average coercivities (Bh) of the three phases are ~10, ~154 and ~1550 (red) or 2350 (green) mT. IRM deconvolution suggests that magnetite (~65%) and pyrrhotite (~35%) are dominant in the green sediments. The demagnetization of three-axis IRM (Lowrie, 1990) shows: (1) predominance of the soft component and relatively less represented moderate/hard component, with green samples demagnetized at 580°C; (2) predominance of the moderate/hard component, that completely loses magnetization at 660°C in the red samples; (3) mixed behaviour in the mixed colour samples. Furthermore, the moderate and soft components show a drop of magnetization between 100°C and 200/250°C.

The AF demagnetization of the green sediment occurs at lower fields (median destructive field, MDF ~ 13.3 mT) than in the red sediment (MDF ~ 19.5 mT). A small fraction of this NRM is drilling-induced magnetization, characterized by an anomalously steep magnetization ($I > 75°$ instead of $I \sim 26°$ as expected based on paleolocation). Between 20 and 60 mT, the behaviour of the green sediment contrasts with the tendency of red samples to retain magnetization. Remarkably, during AF demagnetization experiments, some of the green sediments exhibit an overall gain in magnetization above 70 mT interpreted as gyromagnetic remanence, a property of pyrrhotite, and greigite (Stephenson & Snowball, 2001; Thomson, 1990). In the green sediments, the saturation IRM to magnetic susceptibility ($SIRM/\chi$) ratio (Larsen, Jian, et al., 2018), as shown by Snowball (1991) elsewhere, is too low for greigite.

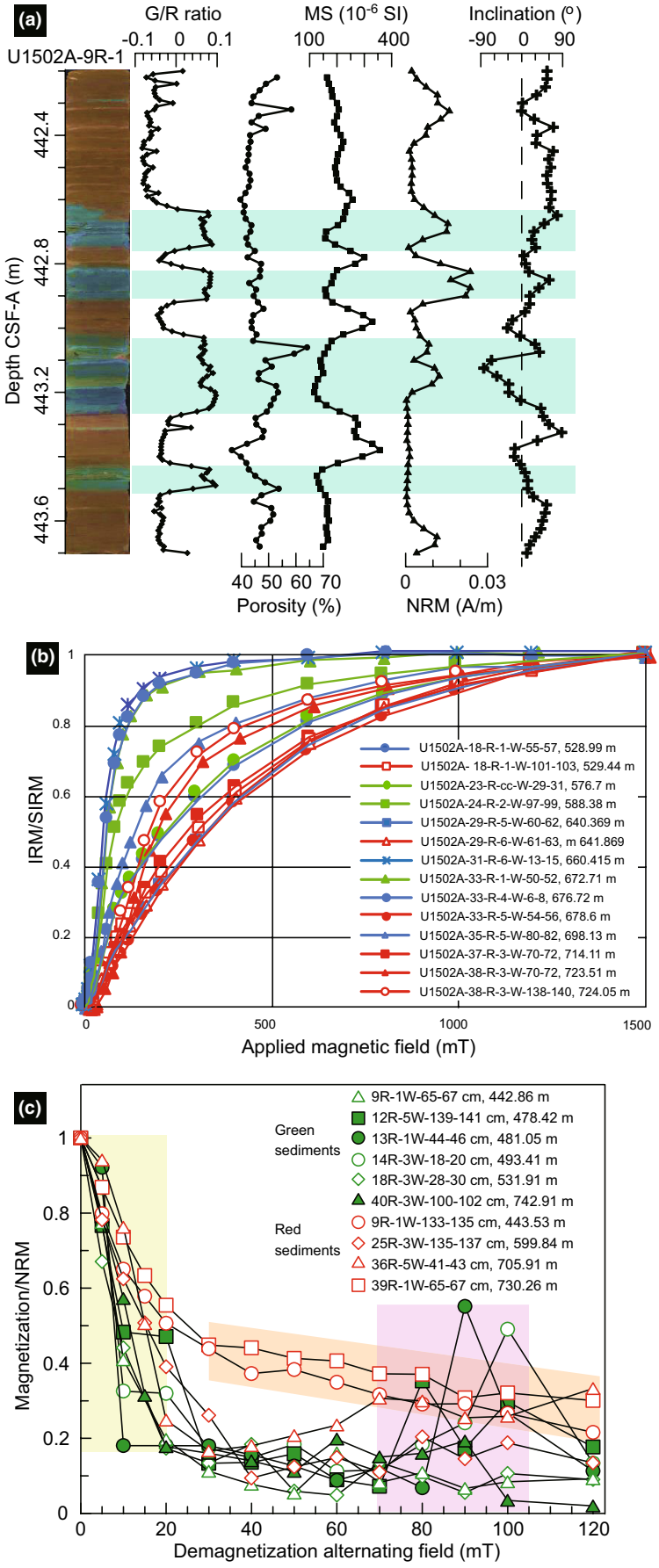

FIGURE 3 (a) Example of petrophysical and magnetic data from IODP Hole U1502A drill cores, from left to right: colour image of the core; bimodal green/red ratio measured from the spectral analysis; high porosity spatially correlated with green zones; low magnetic susceptibility correlated with green zones (replacement of magnetite by pyrrhotite), high NRM intensities correlated with green zones, and inclination anomalies correlated with green zones. (b) Behaviour of red and green sedimentary rocks in normalized isothermal remanent magnetization acquisition curves. The red sediments (red symbols) host a magnetically hard phase (haematite), whereas the green sediments (green symbols) show a magnetically soft phase (pyrrhotite); mixed colour samples with red and green sediments (blue symbols) show a mixed behaviour. (c) Normalized alternating field demagnetization of the NRM, showing three behaviours: pyrrhotite-magnetite (yellow), haematite (orange) and pyrrhotite (purple) dominated assemblages.

5 | POST-DEPOSITIONAL ALTERATION MODEL

From 660 to 740 m (Cores 32R to 39R; Figures 2 and S1), the sediments display a brownish-red colour with a few green patches (reduction spots and haloes along fractures). From 375 to 660 m (Cores 2R to 31R; Figure S1), the sediments show coarse-grained, stratiform and high porosity intervals ranging from a few millimetres to tens of centimetres, interpreted as turbidites (Larsen, Jian, et al., 2018).

In the lower part of the drill hole, green reduction spots in an otherwise reddish material attest to the presence of reducing material that reacted with the sediment during and after diagenesis. These reduction spots could have resulted from microbial activity (Spinks et al., 2010) or trapped sulfides (Hofmann, 1990). The presence of abundant sulfides, including pyrrhotite, both in the basaltic stockwork underlying the Miocene sedimentary unit and in the greenish beds above is supported by shipboard thermal demagnetization experiments (Larsen, Jian, et al., 2018) and our results. While the origin of these sulfides in veins crossing the basalts can be attributed to hydromagmatic fluids, a microbial origin cannot be ruled out. The proximity of the stockwork to the greenish beds further supports a common origin for their respective sulfides.

Reduction of haematite to magnetite (reaction 1) and magnetite to pyrrhotite (reaction 2) can take place through the two reactions (e.g., Tarling & Hrouda, 1993):

$$3\,Fe_2O_3 + H_2 \rightarrow 2\,Fe_3O_4 + H_2O \quad (1)$$

$$7\,Fe_3O_4 + 24S \rightarrow 3\,Fe_7S_8 + 14\,O_2 \quad (2)$$

In the lower part of the drill hole, the green zones form stratified intervals, beds and laminae, corresponding to high porosity intervals with five times higher sulfur content than in the surrounding reddish material (Figure S3). In the upper part of the core, the magnetic assemblage of the reddish materials is dominated by haematite, whereas the greenish zones are dominated by magnetite and pyrrhotite (Figure 3b,c). We interpret the presence of pyrrhotite in the green intervals to result from fluids percolating through the higher porosity material with higher permeability. Alternatively, Jin et al. (2020) interpreted the rhythmic reddish-brown and greenish-grey sediments to result from orbitally-driven deep water circulation. We consider this alternative hypothesis less likely because the green intervals present systematic differences in magnetic inclination (Figure 3a), suggesting that their NRM was acquired, at a different time, through post-depositional chemical remanent magnetization. The main evidence for the greenish colour of the sediments resulting from post-depositional fluids is the widespread geometrical unconformity between the green-coloured zones with respect to bedding (Figure 2). The systematic greenish colour of turbiditic zones that also have a coarser grain size and higher permeability strongly also supports this interpretation. The rhythmicity was not remarkable at nearby IODP Sites U1501 and U1505 (Jin et al., 2020). This supports a local- rather than basin-wide origin for the sediment colour at U1502.

We propose that sulfur-rich fluids responsible for the precipitation of pyrrhotite (and magnetite) in these green intervals may have been sourced from the basalts underlying the sedimentary units of Hole U1502A (Figure 1b). These basalts are extensively altered by hydrothermal fluids and are crisscrossed by a dense sulfide stockwork (up to 32% volume of sulfides; Larsen, Jian, et al., 2018). Supporting this interpretation is the coincidence between the depth at which the sedimentary core shows the pervasive sulfur-rich fluid flow and the depth of the basement top (Figure 4). Our interpretation fits well with the models of basinal fluid flow between recharging and discharging seamounts of Fisher and Wheat (2010) and recent heat flow modelling for the

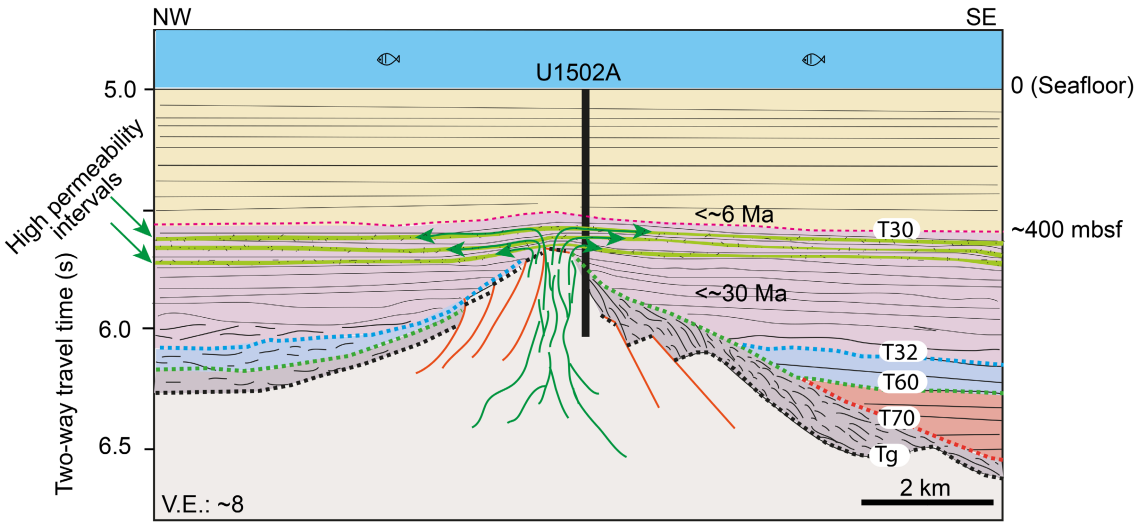

FIGURE 4 Interpreted seismic profile schematically showing the spatial correlation between green sediments and the stratigraphic height where reducing fluids would be expected to be discharged.

area (Nirrengarten et al., 2020). Alternatively, sulfur-rich fluids could be trans-basinal brines unrelated to the sulfide-rich basement highs. The latter hypothesis, however, is not supported by the lack of greenish alteration zones in the other holes drilled in the basin during IODP Expeditions 367/368.

Ocean scientific drilling and other fields of subsurface exploration generally view redox conditions during early diagenesis as the result of early depositional environments, and generally representative of the two main near-surface reservoirs, i.e., ocean and atmosphere. This view in turn influences how organic carbon preservation, sulfur cycling (Morse & Berner, 1995), and oxygen cycling (Kasting, 2001) are interpreted; except where hydrothermal processes have direct surface expression, deep crustal processes seem undetectable. However, in this case of Hole U1502, a low-temperature but long-acting hydrothermal system (Fisher & Wheat, 2010) of a type not uncommon to medial and distal rift systems, has coupled fluid-driven processes in the basement and overlying sedimentary layers. Such system transfers heat to generate hydrocarbons (Waples, 1980), and supplies reductants important to the deep biosphere and capable of oxidizing hydrocarbons (Crémière et al., 2016).

6 | CONCLUSION

The interpretation that the colour of sediments reflects syn-depositional redox conditions remains overall valid. Yet, here we show that in ocean basins where hydrothermal circulation is active, the general interpretation of sediment colour needs to be verified by considering the impact of underlying basement through which fluid flow would yield strongly reducing fluids. Post-depositional fluid flow is particularly likely to occur in high-permeability sediments such as turbidites. These post-depositional fluids and their pathways can be detected with magnetic and paleomagnetic methods because the associated assemblages are fundamentally different in the pristine and reduced series. The impact that basement-derived reducing fluids would have on hydrocarbon maturation also needs to be considered.

ACKNOWLEDGEMENTS

Support was provided by Chinese 111 (HW), ECORD (SS), Korean IODP (DC), National Science Foundation (ECF), Natural Environment Research Council (SAB) and U.S. Science Support Program, Lamont-Doherty Earth Observatory (ECF, PP). Marco Maffione, an anonymous reviewer, the Associate Editor and Max Coleman are kindly acknowledged.

DATA AVAILABILITY STATEMENT

The data that support the findings of this study are available from the corresponding author upon reasonable request.

ORCID

S. Satolli https://orcid.org/0000-0001-9848-9745

REFERENCES

Briais, A., Patriat, P., & Tapponnier, P. (1993). Updated interpretation of magnetic anomalies and seafloor spreading stages in the South China Sea: Implications for the Tertiary tectonics of Southeast Asia. *Journal of Geophysical Research: Solid Earth*, *98*(B4), 6299–6328.

Crémière, A., Lepland, A., Chand, S., Sahy, D., Kirsimäe, K., Bau, M., Whitehouse, M. J., Noble, S. R., Martma, T., Thorsnes, T., & Brunstad, H. (2016). Fluid source and methane-related diagenetic processes recorded in cold seep carbonates from the Alvheim channel, central North Sea. *Chemical Geology*, *432*, 16–33. https://doi.org/10.1016/j.chemgeo.2016.03.019

Fisher, A. T., & Wheat, C. G. (2010). Seamounts as conduits for massive fluid, heat, and solute fluxes on ridge flanks. *Oceanography*, *23*(1), 74–78. https://doi.org/10.5670/oceanog.2010.63

Hofmann, B. A. (1990). Reduction spheroids from northern Switzerland: Mineralogy, geochemistry and genetic models. *Chemical Geology*, *81*(1), 55–81.

Jian, Z., Larsen, H. C., Alvarez Zarikian, C. A., & Expedition 368 Scientists. (2018). Expedition 368 preliminary report: South China Sea rifted margin. *International Ocean Discovery Program Preliminary Reports*. https://doi.org/10.14379/iodp.pr.14368.12018

Jin, X., Xu, J., Li, H., Li, Y., Qiao, P., Wu, L., Ling, C., Li, B., & Liu, C. (2020). Origin of the rhythmic reddish-brown and greenish-gray sediments in the abyssal South China Sea: Implications for oceanic circulation in the late Miocene. *Marine Geology*, *430*, 106378.

Kasting, J. F. (2001). The rise of atmospheric oxygen. *Science*, *293*, 819–820.

Larsen, H. C., Jian, Z., Alvarez Zarikian, C. A., Sun, Z., Stock, J. M., Klaus, A., Boaga, J., Bowden, S. A., Briais, A., Chen, Y., Cukur, D., Dadd, K. A., Ding, W., Dorais, M. J., Ferré, E. C., Ferreira, F., Furusawa, A., Gewecke, A. J., Hinojosa, J. L., … Zhong, L. (2018). Site U1502. In Z. Sun, Z. Jian, J. M. Stock, H. C. Larsen, A. Klaus, C. A. Alvarez Zarikian, & the Expedition 367/368 Scientists (Eds.), *South China Sea rifted margin. Proceedings of the International Ocean discovery program*, *367/368*. International Ocean Discovery Program. https://doi.org/10.14379/iodp.proc.367368.367106.362018

Larsen, H. C., Mohn, G., Nirrengarten, M., Sun, Z., Stock, J., Jian, Z., Klaus, A., Alvarez-Zarikian, C. A., Boaga, J., Bowden, S. A., Briais, A., Chen, Y., Cukur, D., Dadd, K., Ding, W., Dorais, M., Ferré, E. C., Ferreira, F., Furusawa, A., … Zhong, L. (2018). Rapid transition from continental breakup to igneous oceanic crust in the South China Sea. *Nature Geoscience*, *11*(10), 782–789.

Liu, Q., Roberts, A. P., Larrasoaa, J. C., Banerjee, S. K., Guyodo, Y., Tauxe, L., & Oldfield, F. (2012). Environmental magnetism: Principles and applications. *Reviews of Geophysics*, *50*, RG4002. https://doi.org/10.1029/2012RG000393

Lowrie, W. (1990). Identification of ferromagnetic minerals in a rock by coercivity and unblocking temperature properties. *Geophysical Research Letters*, *17*(2), 158–162. https://doi.org/10.1029/GL017i002p00159

Maxbauer, D. P., Feinberg, J. M., & Fox, D. L. (2016). MAX UnMix: A web application for unmixing magnetic coercivity distributions. *Computers and Geosciences*, *95*, 140–145. https://doi.org/10.1016/j.cageo.2016.07.009

Morse, J. W., & Berner, R. A. (1995). What determines sedimentary C/S ratios? *Geochimica et Cosmochimica Acta*, *59*(6), 1073–1077. https://doi.org/10.1016/0016-7037(95)00024-T

Nirrengarten, M., Mohn, G., Schito, A., Corrado, S., Gutiérrez-García, L., Bowden, S. A., & Despinois, F. (2020). The thermal imprint of continental breakup during the formation of the South China Sea. *Earth and Planetary Science Letters*, *531*, 115972. https://doi.org/10.1016/j.epsl.2019.115972

Pautot, G., Rangin, C., Briais, A., Tapponier, P., Benzart, P., Lericolais, G., Mathieu, X., Wu, J., Han, S., Li, H., Lu, Y., & Zhao, J. (1986). Spreading direction in the central South China Sea. *Nature*, *321*, 150–154.

Snowball, I. F. (1991). Magnetic hysteresis properties of greigite (Fe_3S_4) and a new occurrence in Holocene sediments from Swedish Lappland. *Physics of the Earth and Planetary Interiors*, *68*(1–2), 32–40.

Spinks, S. C., Parnell, J., & Bowden, S. A. (2010). Reduction spots in the Mesoproterozoic age: Implications for life in the early terrestrial record. *International Journal of Astrobiology*, *9*(4), 209–216.

Stephenson, A., & Snowball, I. F. (2001). A large gyromagnetic effect in greigite. *Geophysical Journal International*, *145*(2), 570–575.

Tarling, D., & Hrouda, F. (1993). Magnetic anisotropy of rocks. In *Springer Science & Business Media* (p. 230). Chapman & Hall.

Thomson, G. F. (1990). The anomalous demagnetization of pyrrhotite. *Geophysical Journal International*, *103*(2), 425–430.

Waples, D. W. (1980). Time and temperature in petroleum formation: Application of Lopatin's method to petroleum exploration. *AAPG Bulletin*, *64*(6), 916–926. https://doi.org/10.1306/2F9193D2-16CE-11D7-8645000102C1865D1980

SUPPORTING INFORMATION

Additional supporting information can be found online in the Supporting Information section at the end of this article.

Data S1.

How to cite this article: Ferré, E. C., Satolli, S., Wu, H., Persaud, P., Çukur, D., & Bowden, S. A. (2023). Red or green: Overprinting of the climatic signal in Miocene sediments, South China Sea (IODP Expedition 368, Site U1502). *Terra Nova*, *00*, 1–8. https://doi.org/10.1111/ter.12670